

## Supplementary Information

### Minimally invasive spin sensing with scanning tunneling microscopy

*Luigi Malavolti,<sup>1,2,3</sup> Gregory McMurtrie,<sup>1,2,3</sup> Steffen Rolf-Pissarczyk,<sup>2,3</sup> Shichao Yan,<sup>2,3,4</sup> Jacob A. J. Burgess,<sup>2,3,5</sup> and Sebastian Loth<sup>1,2,3</sup>*

<sup>1</sup>Institute for Functional Matter and Quantum Technologies, University of Stuttgart, 70569 Stuttgart, Germany

<sup>2</sup>Max Planck Institute for the Structure and Dynamics of Matter, 22761 Hamburg, Germany

<sup>3</sup>Max Planck Institute for Solid State Research, 70569 Stuttgart, Germany

<sup>4</sup>School of Physical Science and Technology, ShanghaiTech University, Shanghai 201210 China

<sup>5</sup>Department of Physics and Astronomy, University of Manitoba, Winnipeg, Manitoba, Canada R3T 2N2

#### **S1) Pump probe measurements**

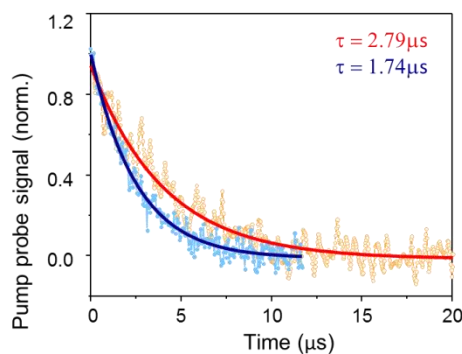


**FIG. S1:** Pump probe decay curves acquired at 0.75 T and 2 T field in +Z (Fig. S6), pale blue and orange respectively, along with fitting curves. The decay time  $\tau$  of each curve is reported in the top right corner of the figure.

## S2) Correlation plot

In order to correlate the telegraph noise in the conductance signal with the switching of the nano-AF states, we quickly alternated between remote and direct measurements. The observed height of the nano-AF's atom, at the moment of transitioning from remote to direct measurement, links the nano-AF's Néel-like states to the conductance state of the sensor spin (Fig. S2). We repeated this procedure 26 times and found a consistent correlation between conductance level and apparent height signal.

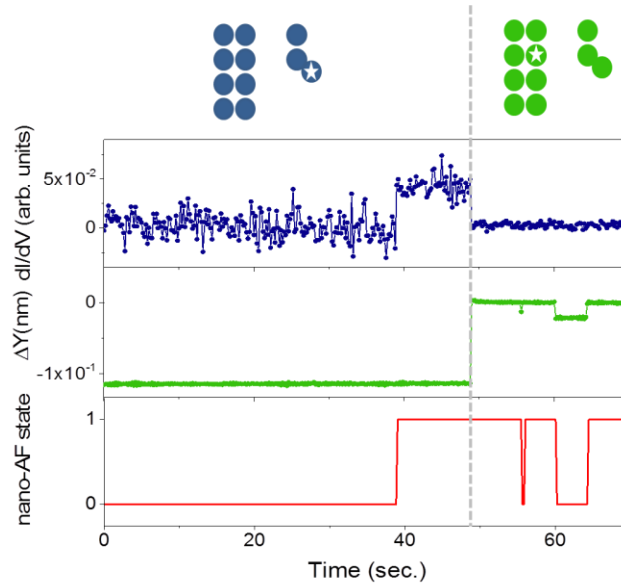


**FIG. S2:** Procedure used to correlate the nano-AF state and the sensor conductance. The lockin signal is reported in blue, the relative tip-surface distance in green, and the reconstructed state of the nano-AF in red. Initially, the tip is positioned over the third atom of the sensor, as in the top left cartoon, at a bias of -5.2 mV and a modulation bias of 720  $\mu$ V. In this position the lockin signal provides information about the conductance of the sensor. No information is encoded in  $\Delta Y$ . The jump in the  $dI/dV(V)$  signal at around 40 s indicates a switch of the nearby nano-AF. At around 50 s (grey dotted line), the tip is rapidly moved from the sensor to the nano-AF, to the position shown in the cartoon on the top right. No changes are applied to the bias or the current. In this position the lockin signal provide no useful information, while  $\Delta Y$  allows the switching of the nano-AF to be monitored.

### S3) Signal to noise ratio

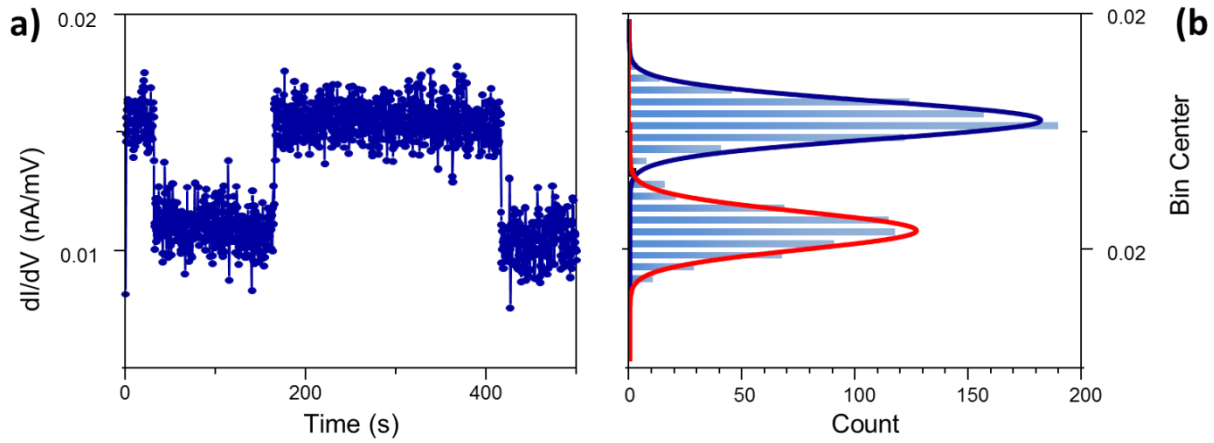


**FIG. S3:** (a) Trace of two level noise in the differential conductance recorded with the tip over the sensor (third atom, 125 pA current, -5.2 mV bias, 720  $\mu$ V AC modulation). (b) Signal distribution of the trace presented in (a) along with the two Gaussian fits; the same standard deviation is imposed to the two distributions. The distance between the centers of the two Gaussian curves defines the measured signal; the standard deviation defines the noise of the measurement. The data presented here is a subset of the complete dataset, as such this is not representative of this specific current set point.

#### S4) Fit of the signal to noise current dependence

The noise in the sensor measurement depends linearly on the current. The dependence was obtained from a fit of the experimental data (Fig. S4). The noise data points were obtained as described in Section 3.

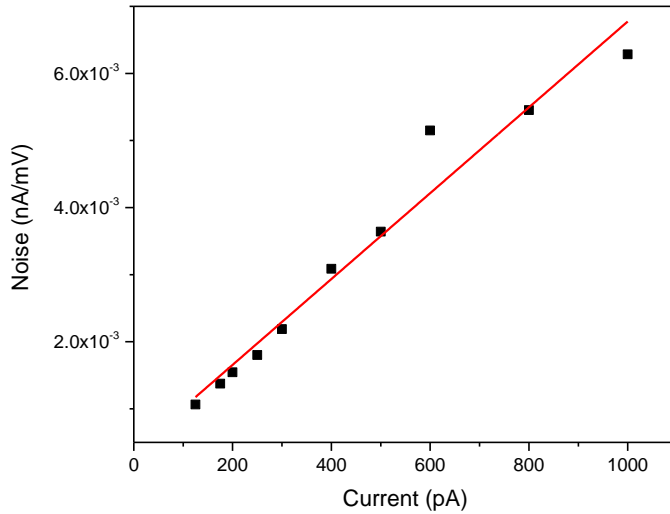


**FIG. S4:** Current dependence of the sensor measurement noise (black square) along with a linear fit (red line).

The signal in the sensor measurement also depends on the current. The current dependence of the signal is proportional to the degree of coupling between the nano-AF and the sensor. Using this coupling as a fit parameter allows the current dependence to be described using the model from section 5. Combining this with the fitted noise dependence yields the signal/noise fit presented in Fig.3b of the main text.

The interaction is accounted by an effective magnetic field  $\delta B = 0.1\text{T}$  experienced by the first and second atom. In an external magnetic field of  $B_e = 2.0\text{ T}$ , the atoms 1 and 2 experience a magnetic field  $B_0 = B_e + \delta B$  for nano-AF in state 0 and a magnetic field  $B_1 = B_e - \delta B$  for nano-AF in state 1.

The third atom of the sensor is expected to not be influenced by a local field due to symmetry arguments (see section 6). The  $u$  parameter, and the  $\eta$  parameter (which account for the spin polarization of the tip) are also allowed to vary, see Table S1.

**Table S1:** Parameters used for the fitting of the signal to noise graph. Parameters which define the spin Hamiltonian of the sensor are fixed (see also Table S2).

	Atom 1 and 2	Atom 3
$\delta B$ (T)	0.1	0.0
$B_0$ (T)	2.1	2.0
$B_1$ (T)	1.9	2.0
$u$	0.30	$\eta^{*})$ 0.53

<sup>\*)</sup>This parameter accounts for the spin polarization of the tip

Simulated  $dI/dV(V)$  spectra, using the parameters obtained from this fit, are reported in Fig. S5. The signal is the difference between the two spectra at the measurement bias (-5.2 mV).

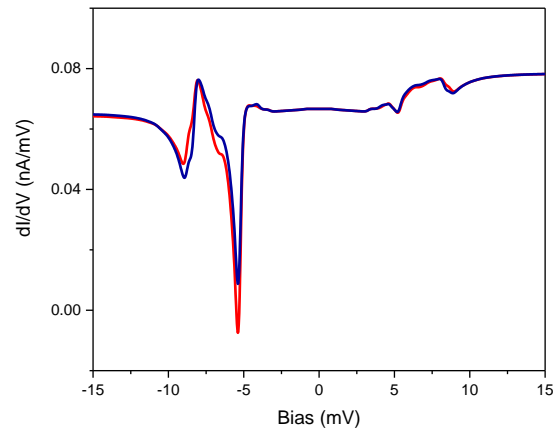


**FIG. S5:** Simulated spectra for the third atom of the sensor when the nano-AF is in state 0 (blue) and state 1 (red). Junction setpoint of 15 mV, 1 nA.

### S5) Fitting procedure

We model the three-Fe-atom sensor spin with an effective spin Hamiltonian of the form:

$$H = J_{(12)}\vec{S}_{(1)} \cdot \vec{S}_{(2)} + J_{(23)}\vec{S}_{(2)} \cdot \vec{S}_{(3)} + \sum_i \left[ g\mu_B\vec{S}_{(i)} \cdot \vec{B}_{(i)} + D_{(i)} \cdot \hat{S}_{z(i)}^2 + E_{(i)}(\hat{S}_{y(i)} - \hat{S}_{x(i)})^2 \right]$$

where  $\mu_B$  is the Bohr constant,  $g$  is the g-factor,  $J_{(12)}$  and  $J_{(23)}$  are the exchange coupling between the first and second atom and the second and third atom, respectively. The interaction between the first and third atom of the sensor was neglected.  $\vec{S}_{(i)}$ ,  $D_{(i)}$  and  $E_{(i)}$  are the spin vector operator, the uniaxial anisotropy parameter and the transverse anisotropy parameter of the  $i$ th Fe atom.  $\hat{S}_{x(i)}$ ,  $\hat{S}_{y(i)}$ , and  $\hat{S}_{z(i)}$  are the  $x$ ,  $y$  and  $z$  components of  $\vec{S}_{(i)}$  (the coordinate system is shown in Fig. S6). The spin eigenstates are obtained by diagonalizing  $H$ .

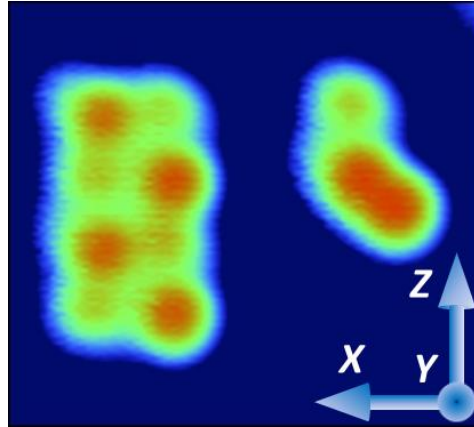


**FIG. S6:** Spin contrast STM image of the nano-AF, along with the sensor spin positioned at a distance of 1.9 nm and the reference coordinate system (tunnel junction setpoint 4 mV, 5 pA).

Tunneling electrons interact with the Fe atoms and induce transitions between the spin eigenstates. These, in turn, modify the transition probability for electron tunneling between tip and sample. We model the interaction between electrons and Fe atoms as spin-dependent exchange scattering of the form  $\vec{S} \cdot \vec{\sigma} + u$  [1,2] where  $\vec{S}$  and  $\vec{\sigma}$  are the spin vector operator of the local spin system and the tunneling electron respectively while  $u$  is a real parameter accounting for spin independent component.

$dI/dV(V)$  spectra are then calculated by a Master equation approach that describes the tunnel current as a result of electron-spin scattering with the sensor. [1,3] Least-squares fitting of the calculated spectra to the experimental data yields quantitative values for the anisotropy and for the coupling between the atoms of the sensor.

In order to obtain the Hamiltonian parameters, the  $dI/dV(V)$  spectrum acquired for the third atoms of the sensor at 2.0 T magnetic field was fitted (Fig. S7). The parameters obtained are reported in table S2.

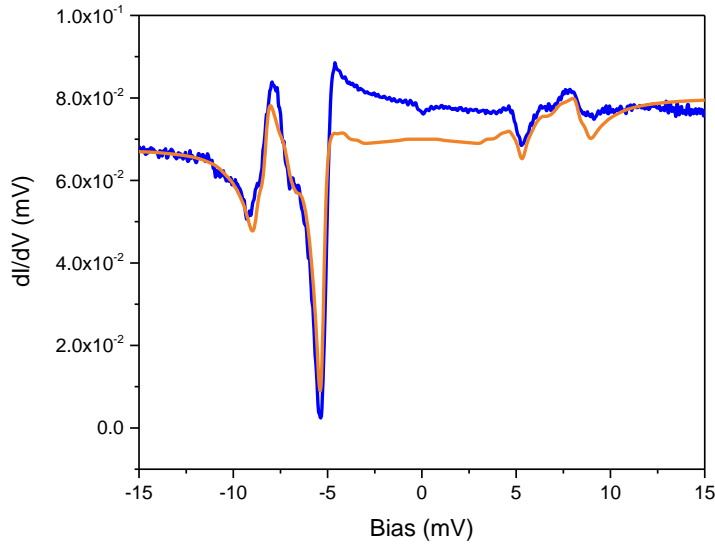


**FIG. S7:**  $dI/dV(V)$  spectra acquired with the tip over the third atom of the sensor at 2 T magnetic field (blue line) and its fit (orange line). Junction setpoint: -15 mV, 1 nA.

**Table S2:** Hamiltonian parameters obtained by fitting the spectrum of the third atom acquired at 2 T magnetic field.

	<b>Atom 1</b>	<b>Atom 2</b>	<b>Atom 3</b>
<b>D</b> (meV)	<i>-1.92</i>	<i>-1.80</i>	<i>-1.54</i>
<b>E</b> (meV)	<i>0.22</i>	<i>0.21</i>	<i>0.29</i>
<b>J<sub>1-2</sub></b> (meV)	<i>0.71</i>	<b>J<sub>2-3</sub></b> (meV)	<i>-0.56</i>
<b>u</b>	<i>0.55</i>	<b><math>\eta^*</math></b>	<i>0.39</i>

<sup>\*</sup>This parameter accounts for the spin polarization of the tip

### S6) Symmetry considerations for the nano-AF–Sensor interactions

The geometry of the nano-AF on the  $\text{Cu}_2\text{N}$  surface exhibits two symmetry planes, as shown in Fig. S8. When the magnetic moment of the atoms is considered, the two planes describe an anti-symmetric operation for both the two Néel-like states. The magnetic interaction between the nano-AF and objects featuring such a symmetry plane is thus expected to cancel out. This is the case of the third atom of the sensor. As such, no variation of the local magnetic field is expected to directly affect such an atom when the nano-AF switches from one to the other Néel state. A different situation is expected for the other atoms constituting the sensor. In their positions, the magnetic interaction is expected to mediate to a finite value.

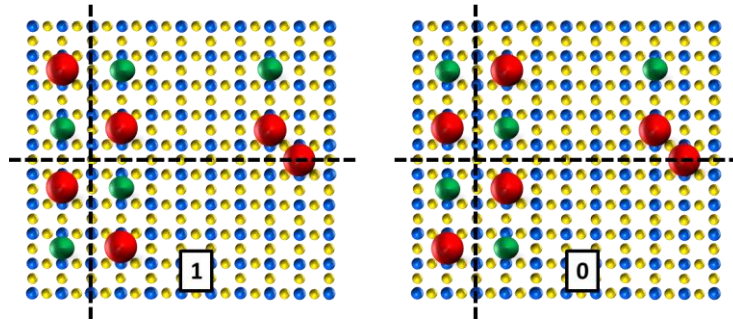


**FIG. S8:** Schematic representation of the two nanostructures on the  $\text{Cu}_2\text{N}$  surface. Color scheme: Cu yellow, N blue. The Fe atoms are red for atoms with their magnetic moment parallel to the external magnetic field and green for atoms with their magnetic moment antiparallel to the field. The two dashed lines indicate the two anti-symmetric plane operations for the nano-AF.

**S7) Current dependence occupation probability using direct inspection**

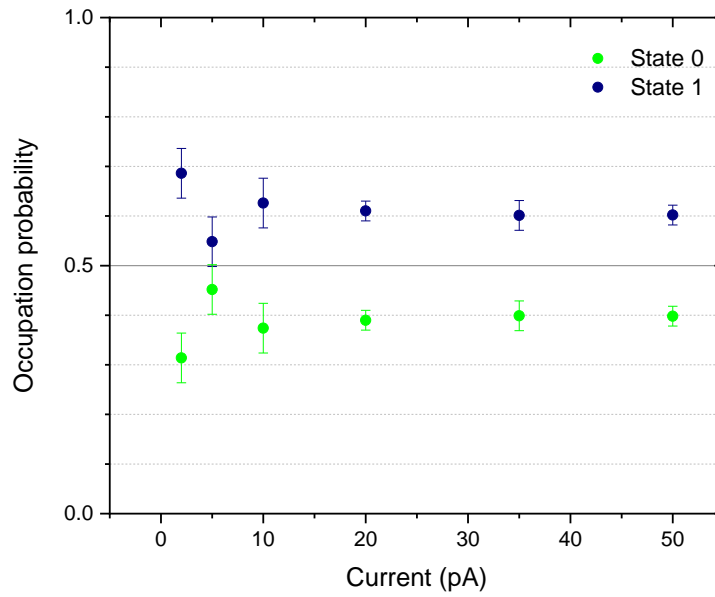


**FIG. S9:** Time-averaged occupation of the two nano-AF states ‘0’ and ‘1’ for direct measurement with the tip positioned over the nano-AF as depicted in central panel of Fig.4a main text (data acquired using bias setpoint of -5.2 mV and 5.2 mV). No current dependent trend is observed.

### S8) Current dependence occupation probability using remote measurement

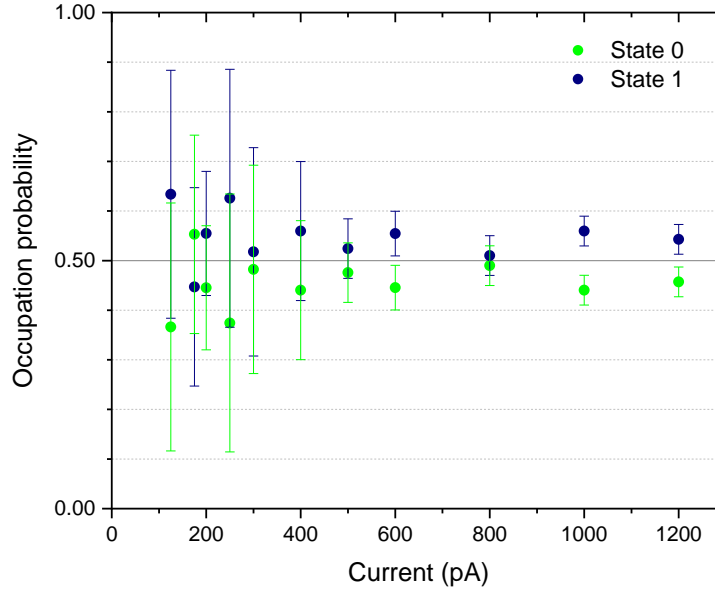


**FIG. S10:** Time-averaged occupation of the two nano-AF states ‘0’ and ‘1’ for indirect measurement with the tip positioned over sensor (bias setpoint -5.2 mV). No current dependent trend is observed.

### S9) Power law fit parameters

**Table S3:** Result of the power-law fit using the function described in the main text.

	<b>0 to 1</b>	<b>1 to 0</b>	<b>0 to 1 sensed</b>	<b>1 to 0 sensed</b>
<b>Color in Fig. 4 main</b>	<i>Red</i>	<i>Orange</i>	<i>Dark blue</i>	<i>Light blue</i>
<b><math>m</math> (<math>s^{-1}pA^{-\alpha}</math>)</b>	0.027±0.001	0.018±0.001	$1 \cdot 10^{-8} \pm 1 \cdot 10^{-8}$	$1 \cdot 10^{-8} \pm 1 \cdot 10^{-8}$
<b><math>\alpha</math></b>	1.0*	1.0*	2.60±0.21	2.57±0.25
<b><math>r_0</math> (<math>s^{-1}</math>)</b>	0.013±0.010	0.013±0.010	0.013±0.010	0.013±0.010

\*These values were fixed

- [1] S. Loth, C. P. Lutz, and A. J. Heinrich, *New J. Phys.* **12**, 125021 (2010).
- [2] S. Loth, K. von Bergmann, M. Ternes, A. F. Otte, C. P. Lutz, and A. J. Heinrich, *Nat. Phys.* **6**, 340 (2010).
- [3] S. Rolf-Pissarczyk, S. Yan, L. Malavolti, J. A. J. Burgess, G. McMurtrie, and S. Loth, *Phys. Rev. Lett.* **119**, 217201 (2017).